Metallography, Microstructure, and Analysis (2023) 12:1047–1054
https://doi.org/10.1007/s13632-023-01016-3

ORIGINAL RESEARCH ARTICLE

Alternative Reagent for Revealing the Entire Microstructure of Additive Manufactured Ti–6Al–4V Alloy

Ahad Shafiee[1] · Hadi Ghasemi-Nanesa[1] · Mahdi Habibnejad-Korayem[2] · Philippe Bocher[1]

Received: 29 June 2023 / Revised: 18 September 2023 / Accepted: 12 October 2023 / Published online: 20 November 2023

Abstract

The conventional Kroll and Keller's reagents do not reveal uniformly additive manufactured Ti–6Al–4V microstructures, as etching is not uniform over the surface and only detailed electron back scattering diffraction analyses can reveal the details in the microstructures. In this research, an alternative etching solution has been proposed to reveal the microstructures of additive manufactured Ti–6Al–4V. The alternative reagent, never reported for titanium alloys, is known to be efficient for steel microstructures. It is a basic water-based solution containing NaOH and $NaNO_3$ operational at 90 °C for a holding time of up to 30 s. Similar regions of martensitic microstructures generated in 3D-printed parts using laser powder bed fusion were etched by various reagents and compared. The alternative reagent provides optical image resolution at least one order of magnitude superior to the ones obtained with the conventional reagents. It is particularly efficient at revealing as-built martensitic microstructures and can reveal very fine features down to 0.70 µm. Such precise observation provides valuable information on microstructure evolution after heat treatments or hot isostatic pressing.

Keywords Laser powder bed fusion · Titanium alloys · Microstructure · Chemical etching · Hot iso-static pressing · Martensitic structure

Introduction

The arrival of the Ti–6Al–4V alloy in 1954 was a breakthrough thanks to good producibility and its excellent combination of properties. Nowadays, this alloy is still the most widely used titanium alloy in the world, constituting half of titanium products [1]. With a low density, high corrosion resistance, and biocompatibility, Ti–6Al–4V is widely used as hard tissue replacements in artificial bones, joints, and dental implants [2, 3]. In recent years, this alloy was the most popular for the development of additive manufacturing (AM) of metallic parts, and many processes have now reached maturity for the printing of reliable dense parts [4, 5]. In particular, the laser powder bed fusion (L-PBF) technique is the most popular as it uses a laser beam and metallic powders to produce parts with complex geometries that are now used in the field of biomedical and aerospace applications [1, 6, 7].

Analyzing and understanding the microstructure provides valuable insights into the properties, performance, and behavior of Ti–6Al–4V [8–10]. In the conventional classification of titanium alloys, Ti–6Al–4V is an $\alpha + \beta$ titanium dual phase alloy which has an excellent combination of strength and ductility compared with α, quasi α, quasi β, or β phase alloys [11]. The size, morphology, and the arrangement of the two phases, α and β, define the microstructure and properties of Ti–6Al–4V, which are controlled by the thermomechanical history of the material, and in particular by the cooling rate from phase β (the β transus is typically around 995 °C [12]). Rapid cooling generates a supersaturated α' martensitic microstructure and almost no diffusion of elements occurs. Heat treatments in the dual phase region of $\alpha + \beta$ will allow elements and reform a certain percentage of β enriched in vanadium.

The microstructures of Ti–6Al–4V produced by AM processes can be complex, as the material experiences a complex series of heat treatments. For every layer, the high heat input that produces a localized melt pool affects the material that has already been solidified. Layering strategy, process

✉ Ahad Shafiee
ahad.shafiee@etsmtl.ca

[1] Department of Mechanical Engineering, École de technologie supérieure (ÉTS), Québec, Canada

[2] External R&D, AP&C, A GE Additive Company, Québec, Canada

parameters, and the shape and size of the localized melt pool will affect the solidification process as well as the size and intensity of the heat-affected zone. In all cases, the printing process leads to the formation of β columnar grains with various sizes and shapes, which can affect the final microstructure of the printed part [13]. During the printing process under L-PBF, it is estimated that the melt pool is being cooled at a very high rate close to 410 °C/s, leading to a non-equilibrium solidification [14]. As a consequence of this high cooling rate, the microstructure is comprised of a very fine acicular (plate-like) α' martensite, quite different from the bimodal or lamellar $\alpha + \beta$ microstructures produced by conventional manufacturing processes [15].

Revealing the microstructure of printed parts is a key element for understanding the printing process and to properly document the effect of post-heat-treatment processes. For many years, Kroll's reagent [a mixture of hydrofluoric acid (HF) and nitric acid (HNO_3)] and Keller's reagent [a mixture of HF, HNO_3, and hydrochloric acid (HCl)] were successfully used to reveal the microstructures of equiaxed or acicular $\alpha + \beta$ titanium alloys, Widmanstätten, lamellar $\alpha + \beta$, and equiaxed α grain microstructures [11, 14, 16–19]. However, as-built microstructures in [14, 19–22] were poorly revealed by reagents containing hydrofluoric acid and nitric acid, and only backscattered images in scanning electron microscopy (SEM) [23, 24] or electron backscattered diffraction (EBSD) techniques [5] could be used to entirely reveal the microstructural features.

The aim of this work is to share some interesting results obtained during our research with our industrial partner and to propose to the community a promising basic reagent that can reveal small features of martensitic microstructures in an as-built condition.

Materials and Methods

This study was run on cylindrical samples of grade 23 Ti–6Al–4V fabricated through L-PBF technique. The build plate has been considered as the horizontal XY plane, hence, the z-axis is the vertical direction or build direction (BD). The dimensions of the samples were 70 mm × 8 mm and they were printed vertically. The samples were printed using a laser power of 280 W with a spot size of 100 µm. The laser scanning speed, hatch distance, and powder layer thickness were set to 1200 mm/s, 140 µm, and 30 µm, respectively. Three conditions were considered: as-built (AB), heat-treated (HT), and hot isostatic pressed (HIP). The heat treatment was carried out under a protected environment of argon at 900 °C (below the β transus temperature for this alloy) with a soaking time of 1 h followed by furnace cooling. According to ASTM F3001 − 14 [25], the HIP process was performed at 107 MPa and 900 °C for 3 h.

The XZ (parallel to the BD) and XY (perpendicular to the BD) cross-sections of the cylinders were prepared for metallographic examination using standard techniques following by 5 h of vibratory polishing with 0.05-µm colloidal silica. Some micro-harness marks were performed on the surface of the sample using a CLEMEX micro-harness machine to localize the region of interest for microstructural investigation.

The polished samples were etched using three different reagents: Kroll's reagent (2 ml HF, 4 ml HNO_3, and 94 ml H_2O), Keller's reagent (1 ml HF, 2.5 ml HNO_3, 1.5 ml HCl, and 95 ml H_2O), and the proposed basic reagent (40 g NaOH, 15 g $NaNO_3$, 60 g H_2O) introduced by Gouné for steels [26]. This basic reagent is particularly efficient at differentiating bainite from martensite; however, to our knowledge, it has never reported to be used for titanium microstructures. This reagent does not have any specific name, hence, for the sake of ease, it is called "Tichant" in the rest of this paper. While Kroll's and Keller's reagents are used at room temperature typically for 20 s, Tichant reagent is used at 90 °C for 30 s. As water evaporates, its concentration changes and distilled water should be added from time to time to keep the initial composition in place. After applying the Tichant reagent, the sample should be washed only with water and dried with compressed air, i.e., alcoholic solvents such as methanol and ethanol will remove the features created by the reagent. On the other hand, the acidic Kroll's and Keller's reagents etch the sample deeply.

Two as-built samples were etched using Kroll's and Keller's reagents to reveal the microstructure using an OLYMPUS LEXT OLS 4100 confocal microscope. To reveal the potential of the Tichant reagent and to compare the same region after different etching, the microstructures revealed by the Tichant reagent were documented, its features removed by polishing under vibratory conditions, and the same region etched with Kroll's reagent. The obtained images were compared in terms of the α' or α maximum widths for 50 random plates.

Results and Discussion

The microstructure revealed by Kroll's reagent at different magnifications for the AB condition display regions with different gray levels somehow elongated in BD, as illustrated in Fig. 1. Inside these elongated regions, series of parallel lines with specific orientations are found, typical of an acicular martensitic structure. These regions correspond to the columnar structure that solidifies as β grains. They are referred to as prior-β columnar grains, and some of them, particularly well-contrasted, are indicated with yellow arrows in Fig. 1a. Some horizontal wavy lighter lines can be seen across the image which are associated with the

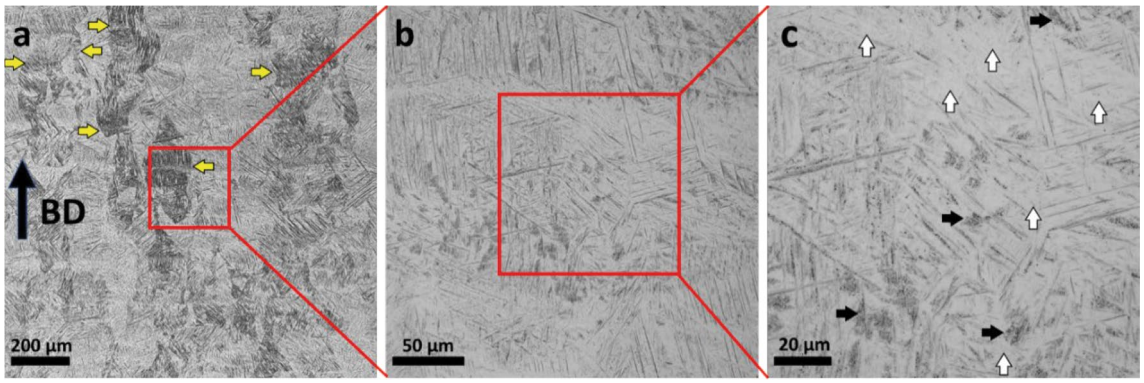

Fig. 1 Microstructure of AB Ti–6Al–4V in XZ plane using fresh Kroll's reagent for 60 s with different magnifications; **a** horizontal lighter layers are barely visible and darker regions are found, some marked with *yellow arrows*, equivalent to prior-β columnar grains; **b** zoom from the center of image *a* showing regions with different contrasts and brightness; and **c** zoom from the center of image *b* showing pitted and unrevealed regions (*dark and white arrows*, respectively) (Color figure online)

built layers. Figure 1b shows that, at higher magnification, it is possible to distinguish some of the acicular grains, but only some of the plates are revealed. It seems that all the lines corresponding to the 12 possible variants can be found in given prior-β grains, but not all the lines are revealed. These variants result from the geometric transformation of the β cubic center phase into the α hexagonal compact phase described by the Burgers orientation relationship [27]. At higher magnification, it becomes evident in Fig. 1c that some regions of the microstructure are not revealed by the reagent, as indicated by the white arrows. A similar microstructure could be seen for the untreated Ti–6Al–4V produced by the selective laser melting (SLM) technique[19]. One could argue that the sample is not sufficiently etched, but in the same image, regions where pitting occurs can be found, identified by the horizontal black arrows. Unetched or pitted regions prevent an adequate documentation of the microstructure, as reported by other researchers on the same material and the same reagent [26, 27]. These over-etched regions were also present in the images taken at intermediate magnification (Fig. 1b). Overall, similar results were found on microstructures revealed by the Keller's reagent, as illustrated in Fig. 2, including the fact that some regions of the microstructure are not revealed, while other regions show some pits. It is relevant to note that the gray-level contrast seen at low magnification is reduced, as higher magnifications are used.

The effect of etching time on the quality of microstructure was further detailed and is reported here for the Kroll's reagent only, but equivalent conclusions can be drawn for Keller's reagent. By increasing the etching time from 20 s to 90 s, it was not possible to reveal the features that were absent while extended pitting occurred in many regions (some of them are shown by dark arrows in Fig. 3). This

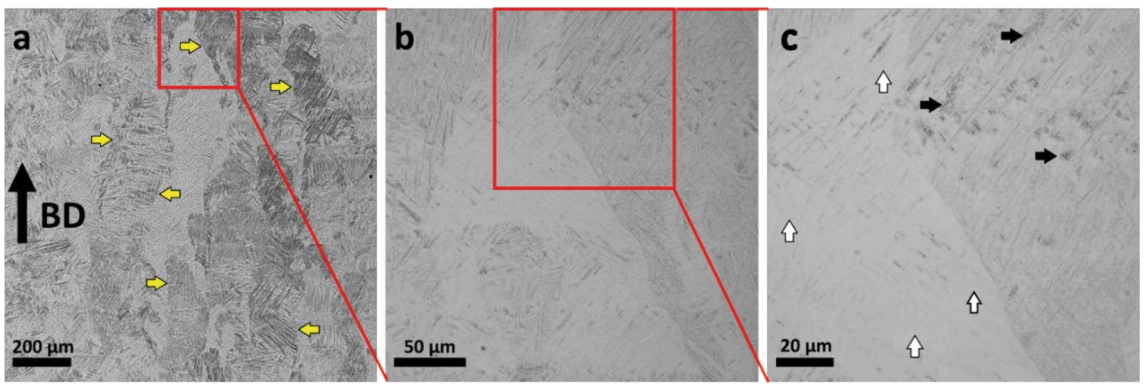

Fig. 2 Microstructure of AB Ti–6Al–4V in XZ plane using fresh Keller's reagent for 60 s with different magnifications; **a** horizontal layers were barely visible and *yellow arrows* indicate the presence of prior-β columnar grains, **b** zoom from the middle–top region of image **a** showing the interface between two areas of different contrasts, and **c** zoom from the middle-top region of image **b** where *dark and white arrows* indicate pitted and unrevealed regions, respectively (Color figure online)

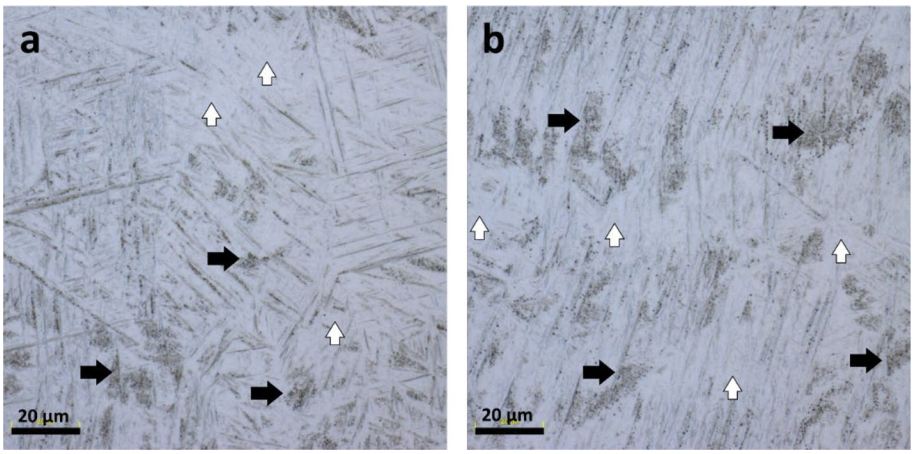

Fig. 3 Microstructure of AB condition of 3D- printed Ti–6Al–4V using Kroll's reagent with different etching times: **a** 60 s and **b** 90 s

means that neither Kroll's nor Keller's reagent can fully reveal the microstructure of the 3D-printed Ti–6Al–4V in the AB condition.

The microstructure in the AB condition, revealed thanks to the Tichant reagent, are spectacular in terms of precision and contrast. Some examples are provided in Figs. 4, 5, 6, and 7 to compare the same microstructure obtained by Kroll's reagent and Tichant reagent. Low and high magnifications are used and the microstructures are examined in the XY and XZ planes. For the XY plane, some dark regions, easily identifiable in Fig. 4a, are surrounded with dashed red curves in Fig. 4b to help the comparison. The regions which could not clearly seen in Fig. 4a, some identified with white arrows, can be distinctly seen in Fig. 4b. Images at higher

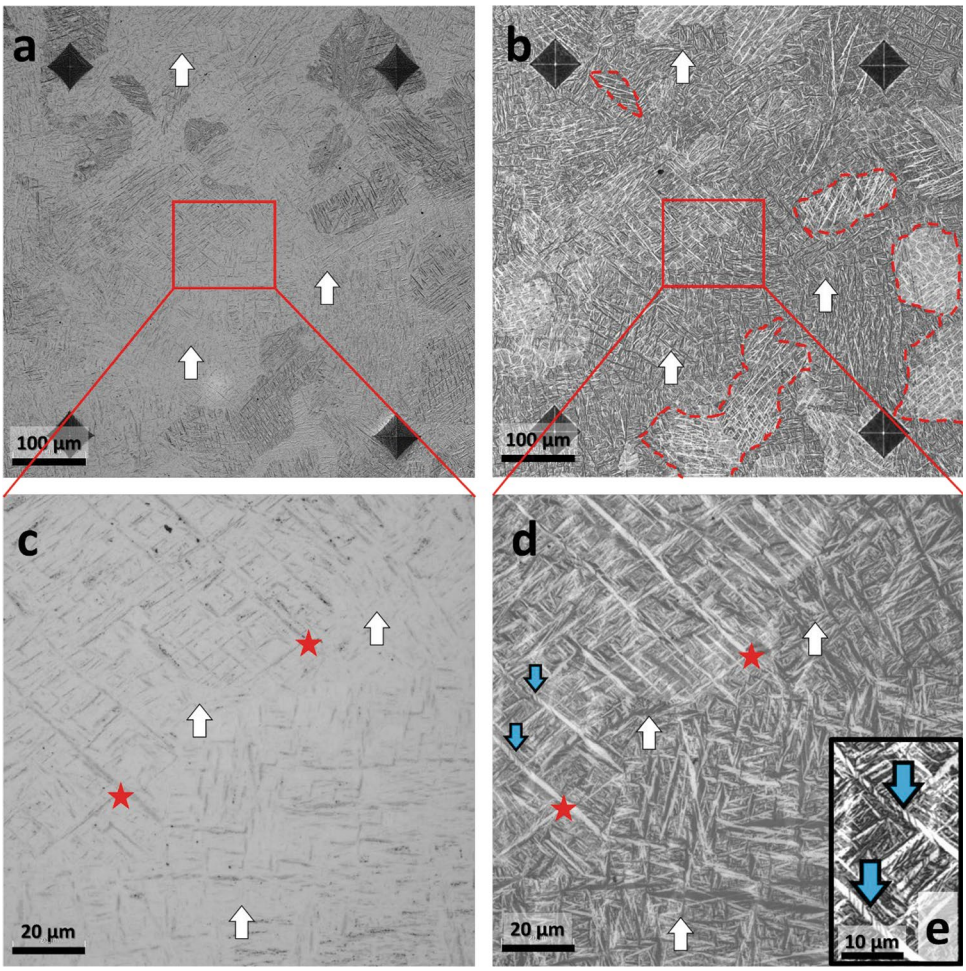

Fig. 4 Microstructure of the AB condition of Ti–6Al–4V in the XY plane using **a**, **c** fresh Kroll's reagent after 30 s and **b**, **d** Tichant reagent for 30 s. White arrows show the regions which could not clearly seen in **a** and **c** and same locations in **b** and **d**. Red stars reflect the same region of interest. The twinning areas are shown with vertical blue arrows and a zoom of this feature is provided in **e** (Color figure online)

magnification were taken in the center of the image and are reported Fig. 4c and d, providing a clear illustration on the precision revealed by the new proposed etching method. Red stars are used to reflect the same region of interest. The microstructure revealed by Kroll's reagent shows some relevant features, but the one revealed by the Tichant reagent bears much more information, showing almost every needle or plate in this area (the white arrows in Fig. 4c and d point to the similar regions). Another interesting point is that the Tichant reagent was able to reveal some mechanical twinning in the thicker martensitic needles. These twinning areas are shown by vertical blue arrows in Fig. 4d. This level of precision is exceptional using optical microscopy. Despite the fully acicular martensitic structure of the AB sample, the Tichant reagent has distinguished different variants of martensite in Fig. 4d, thanks to various gray levels. While it is almost impossible to measure the martensite plate widths in the AB condition for the Kroll's micrograph (Fig. 4c), a value of 0.70 ± 0.40 µm can be calculated for the Tichant micrograph (Fig. 4d). A similar conclusion can be drawn when observing the microstructure in the XY plane, as seen in Fig. 5, and the average martensite plate width as measured for this plane was similar, at 0.67 ± 0.39 µm. The columnar growth parallel to the BD is clearly visible in all regions of the microstructure when using the Tichant reagent, where it is not always possible to differentiate the variation of orientations from one region to the next when Kroll's reagent is used.

Even if Kroll's reagent is known to perform well at revealing the microstructure of heat-treated Ti–6Al–4V, it is relevant to compare the performance of the two reagents for HIP and heat-treated conditions. In both cases, the microstructure becomes larger and a Widmanstätten, lamellar $\alpha + \beta$,structure is found. The nucleation and growth of β phase between the α plates increases the contrast and reveals the morphology of the α phase. Figure 6 shows some typical microstructures after HIP, as revealed using Kroll's and Tichant reagents. The microstructure morphology is well displayed using Kroll's reagent, but it is more or less a binary image where the α phase is white. In particular, it is not possible to differentiate the various variants. The quality of the image obtained using the Tichant reagent is quite impressive in terms of contrast and number of gray levels. In the micrograph produced by the

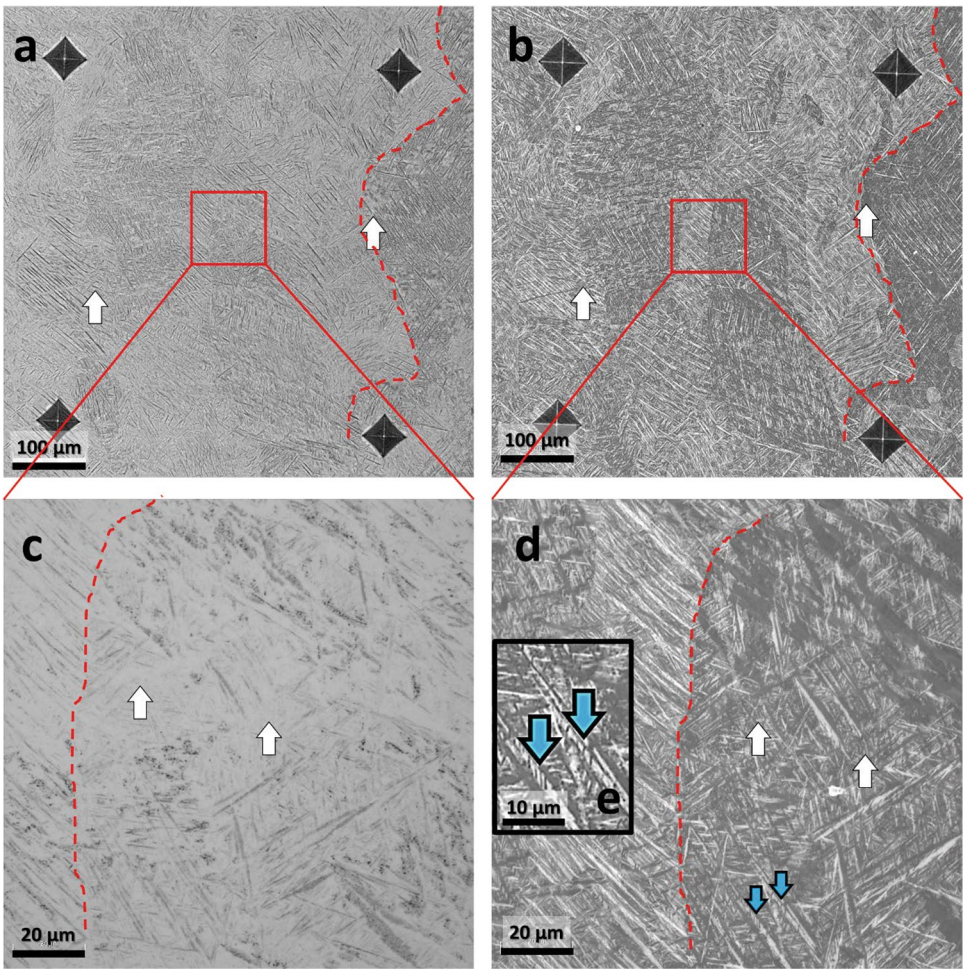

Fig. 5 Microstructure of AB condition of Ti–6Al–4V in XY plane using **a**) and **c**) fresh Kroll's reagent for 30 s and (**b**) and (**d**) Tichant reagent for 30 s. White arrows show the regions which could not clearly seen in **a** and **c** and same locations in (**b**) and (**d**). Red stars reflect the same region of interest. The twinning areas are shown with vertical blue arrows and a zoom of this feature is provided in **e** (Color figure online)

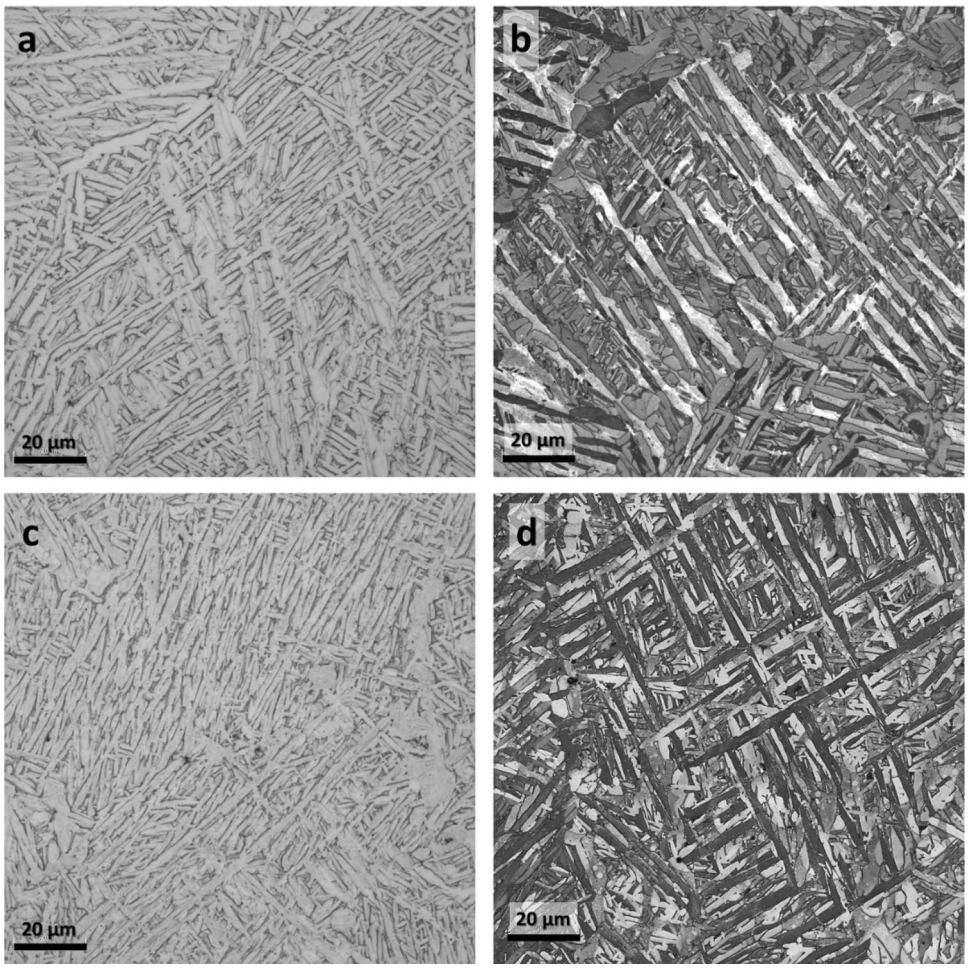

Fig. 6 Microstructure of HIP condition of Ti–6Al–4V in **a** XY plane using Kroll's reagent, **b** XY plane using Tichant reagent, **c** XZ plane using Kroll's reagent, and **d** XZ plane using Tichant reagent. Etching time is 30 s for both reagents

Tichant reagent, many different gray levels can be seen in a given prior-β grain. Slight differences in orientation of these plates may be distinguished by the Tichant reagent and in these various gray levels associated with the different variants. The average α plate widths after HIP process in the XY planes are 1.68 ± 0.66 µm and 1.65 ± 0.35 for the Kroll's and Tichant reagent, and 1.57 ± 0.33 and 1.62 ± 0.52 µm for the XZ planes, respectively.

Since the amount of the β phase for the sample would be less than 10% and the shape of β phase after HIP process is not a plate shape but small islands [28], none of these elongated dark features could be identified as β phase. In the Kroll's reagent micrographs, the α laths, α interface, and small amounts of β, are distinguished by only a two-color contrast. However, when etched with the Tichant reagent, the different variants of the α phase (generated by the various variants of martensitic parents) are revealed with varying levels of gray.

As shown in Fig. 7, the heat-treated samples were held at 900 °C for a shorter time compared to the HIP process and display a similar Widmanstätten lamellar microstructure but with smaller and fragmented features. Again, more features are revealed using the Tichant reagent.

Conclusions

Ti–6Al–4V alloy (grade 23) samples were prepared using the laser powder bed fusion technique. One set of samples were kept in the as-built (AB) condition. A second set of samples were heat treated (HT) at 900 °C for 1 h in an argon atmosphere and hot isostatic pressing (HIP) was applied to some of them at the same temperature but at 107 MPa for 3 h. The microstructures of the AB condition were studied using Kroll's, Keller's, and Tichant reagents and compared. The Tichant reagent is the basic reagent that was used here for the first time to reveal the microstructure of the Ti–6Al–4V alloy. The microstructures of the AB, HT, and HIP conditions were studied using Kroll's and the Tichant reagents and resulting micrographs were compared. It was found that, for the AB condition, Kroll's and Keller's reagents could not reveal

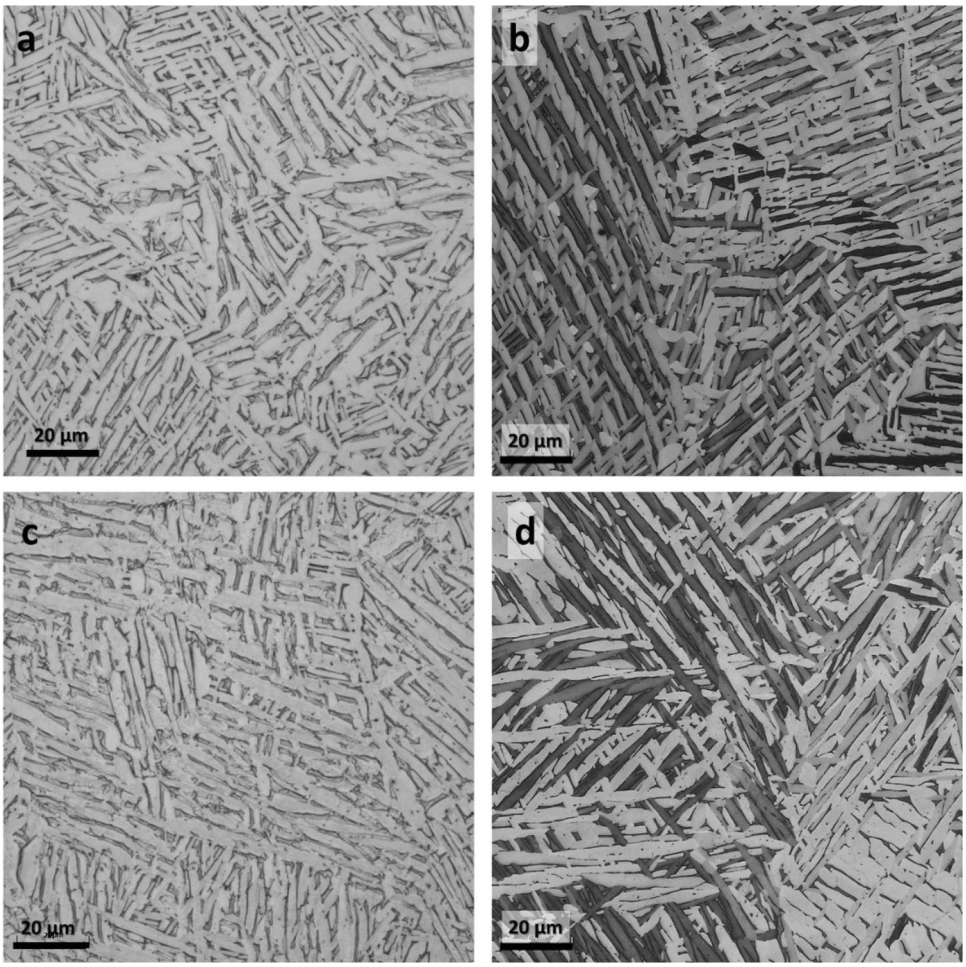

Fig. 7 Microstructure of HT condition of Ti–6Al–4V in **a** XY plane using Kroll's reagent, **b** XY plane using Tichant reagent, **c** XZ plane using Kroll's reagent, and **d** XZ plane using Tichant reagent. Etching time is 30 s for both reagents

the entire microstructure even after longer etching time, while the Tichant reagent could reveal the entire features. All three reagents could reveal the microstructures of the HT and HIP conditions. The Tichant reagent showed more features and more information about the morphology of the microstructure compared with Kroll's and Keller's reagents. In every condition, high-quality micrographs were produced by the Tichant reagent, and the use of this reagent is strongly recommended for titanium alloys, especially for samples manufactured by additive manufacturing techniques, and especially in their as-built condition, as the microstructures produced are thinner due to the higher cooling rate than the conventional method of Ti–6Al–4V manufacturing.

Acknowledgments The authors gratefully acknowledge Amir Hadadzadeh from University of Memphis for printing the samples on which the performance of the etching methods have been demonstrated.

References

1. G. Lütjering, J.C. Williams, *Titanium*, 2nd edn (Springer, Berlin Heidelberg, 2007) https://doi.org/10.1007/978-3-540-73036-1_1
2. C. Cui, B.M. Hu, L. Zhao, S. Liu, Titanium alloy production technology, market prospects and industry development. Mater. Des. **32**, 1684–1691 (2011). https://doi.org/10.1016/J.MATDES.2010.09.011
3. G. Chahine, M. Koike, T. Okabe, P. Smith, R. Kovacevic, The design and production of Ti–6Al–4V ELI customized dental implants. JOM. **60**, 50–55 (2008). https://doi.org/10.1007/S11837-008-0148-2
4. D. Herzog, V. Seyda, E. Wycisk, C. Emmelmann, Additive manufacturing of metals. Acta Mater. **117**, 371–392 (2016). https://doi.org/10.1016/j.actamat.2016.07.019
5. W. Li, K. Zheng, G. Zhao, Y. Zhang, Y. Jin, Variant selection in the thermally treated Ti–6Al–4V processed by laser metal deposition. Metallogr. Microstruct. Anal. (2023). https://doi.org/10.1007/S13632-023-00975-X/FIGURES/6
6. Z.A. Mierzejewska, R. Hudák, J. Sidun, Mechanical properties and microstructure of DMLS Ti6Al4V alloy dedicated to biomedical applications. Materials. **12**, 176 (2019). https://doi.org/10.3390/MA12010176
7. R.E. Śliwa, J. Bernaczek, G. Budzik, The application of direct metal laser sintering (DMLS) of titanium alloy powder in fabricating components of aircraft structures. Key Eng. Mater. **687**, 199–205 (2016). https://doi.org/10.4028/WWW.SCIENTIFIC.NET/KEM.687.199
8. A. Rahimi, M. Shamanian, The PC-GTAW of Ti–6Al–4V thin sheets and its effects on mechanical and microstructural

properties. Metallogr. Microstruct. Anal. **8**, 871–879 (2019). https://doi.org/10.1007/S13632-019-00595-4/FIGURES/11
9. S.R. Al-Sayed, A. Abdelfatah, Corrosion behavior of a laser surface-treated alpha-beta 6/4 titanium alloy. Metallogr. Microstruct. Anal. **9**, 553–560 (2020). https://doi.org/10.1007/S13632-020-00667-W/FIGURES/8
10. Y. Vahidshad, A.H. Khodabakhshi, Effect of solution treatment and aging temperature on α' and Ti3Al(α2) phase formation and mechanical properties of water-quenched Ti–6Al–4V. Metallogr. Microstruct. Anal. **11**, 59–71 (2022). https://doi.org/10.1007/S13632-021-00818-7/TABLES/2
11. M.J. Donachie, *Titanium: a technical guide*, 2nd edn (ASM International, 2000)
12. L.E. Murr, S.A. Quinones, S.M. Gaytan, M.I. Lopez, A. Rodela, E.Y. Martinez, D.H. Hernandez, E. Martinez, F. Medina, R.B. Wicker, Microstructure and mechanical behavior of Ti–6Al–4V produced by rapid-layer manufacturing, for biomedical applications. J. Mech. Behav. Biomed. Mater. **2**, 20–32 (2009). https://doi.org/10.1016/J.JMBBM.2008.05.004
13. R. Shi, S. Khairallah, T.W. Heo, M. Rolchigo, J.T. McKeown, M.J. Matthews, Integrated simulation framework for additively manufactured Ti–6Al–4V: melt pool dynamics, microstructure, solid-state phase transformation, and microelastic response. JOM. **71**, 3640–3655 (2019). https://doi.org/10.1007/S11837-019-03618-1/FIGURES/9
14. T. Ahmed, H.J. Rack, Phase transformations during cooling in $\alpha + \beta$ titanium alloys. Mater. Sci. Eng. A. **243**, 206–211 (1998). https://doi.org/10.1016/s0921-5093(97)00802-2
15. M. Peters, J. Hemptenmacher, J. Kumpfert, C. Leyens, Structure and properties of titanium and titanium alloys. Titan. Titan. Alloy. (2005). https://doi.org/10.1002/3527602119.ch1
16. F.J. Gil, J.M. Manero, M.P. Ginebra, J.A. Planell, The effect of cooling rate on the cyclic deformation of β-annealed Ti–6Al–4V. Mater. Sci. Eng. A. **349**, 150–155 (2003). https://doi.org/10.1016/S0921-5093(02)00784-0
17. I. Weiss, F.H. Froes, D. Eylon, G.E. Welsch, Modification of alpha morphology in Ti–6Al–4V by thermomechanical processing. Metall. Trans. A. **17**, 1935–1947 (1986). https://doi.org/10.1007/BF02644991
18. I. Weiss, D. Eylon, M.W. Toaz, F.H. Froes, Effect of isothermal forging on microstructure and fatigue behavior of blended elemental Ti–6Al–4V powder compacts. Metall. Trans. A. **17**, 549–559 (1986). https://doi.org/10.1007/BF02643962
19. B. Vrancken, L. Thijs, J.P. Kruth, J. Van Humbeeck, Heat treatment of Ti6Al4V produced by selective laser melting: microstructure and mechanical properties. J. Alloys Compd. **541**, 177–185 (2012). https://doi.org/10.1016/j.jallcom.2012.07.022
20. B. Wysocki, P. Maj, R. Sitek, J. Buhagiar, K. Kurzydłowski, W. Święszkowski, Laser and electron beam additive manufacturing methods of fabricating titanium bone implants. Appl. Sci. **7**, 657 (2017). https://doi.org/10.3390/app7070657
21. X. Wang, K. Chou, EBSD study of beam speed effects on Ti–6Al–4V alloy by powder bed electron beam additive manufacturing. J. Alloys Compd. **748**, 236–244 (2018). https://doi.org/10.1016/J.JALLCOM.2018.03.173
22. L. Thijs, F. Verhaeghe, T. Craeghs, J. Van Humbeeck, J.P. Kruth, A study of the microstructural evolution during selective laser melting of Ti–6Al–4V. Acta Mater. **58**, 3303–3312 (2010). https://doi.org/10.1016/j.actamat.2010.02.004
23. W. Xu, E.W. Lui, A. Pateras, M. Qian, M. Brandt, In situ tailoring microstructure in additively manufactured Ti–6Al–4V for superior mechanical performance. Acta Mater. **125**, 390–400 (2017). https://doi.org/10.1016/J.ACTAMAT.2016.12.027
24. S. Cao, Z. Chen, C.V.S. Lim, K. Yang, Q. Jia, T. Jarvis, D. Tomus, X. Wu, Defect, microstructure, and mechanical property of Ti–6Al–4V alloy fabricated by high-power selective laser melting. JOM. **69**, 2684–2692 (2017). https://doi.org/10.1007/S11837-017-2581-6/FIGURES/5
25. ASTM F3001-14, Standard Specification for Additive Manufacturng Titanium-6 Aluminum-4 Vanadium ELI (Extra Low Interstitial) with Powder Bed Fusion, ASTM Standards, 2014, in: n.d.
26. M. Gouné, O. Bouaziz, S. Allain, K. Zhu, M. Takahashi, Kinetics of bainite transformation in heterogeneous microstructures. Mater. Lett. **67**, 187–189 (2012). https://doi.org/10.1016/j.matlet.2011.09.053
27. S.C. Wang, M. Aindow, M.J. Starink, Effect of self-accommodation on α/α boundary populations in pure titanium. Acta Mater. **51**, 2485–2503 (2003). https://doi.org/10.1016/S1359-6454(03)00035-1
28. E. Codaro, R. Nakazato, A. Horovistiz, L.M. Ribeiro, R. Ribeiro, L.R. Hein, An image analysis study of pit formation on Ti–6Al–4V. Mater. Sci. Eng. A. **341**, 202–210 (2003). https://doi.org/10.1016/S0921-5093(02)00218-6